

Micro-patterned molecularly imprinted polymer structures on  
functionalized diamond-coated substrates for testosterone detection

Peer-reviewed author version

KELLENS, Evelien; BOVE, Hannelore; VANDENRYT, Thijs; LAMBRICHTS, Jeroen;  
Dekens, Jolien; DRIJKONINGEN, Sien; D'HAEN, Jan; DE CEUNINCK, Ward;  
THOELLEN, Ronald; JUNKERS, Tanja; HAENEN, Ken & ETHIRAJAN, Anitha (2018)  
Micro-patterned molecularly imprinted polymer structures on functionalized  
diamond-coated substrates for testosterone detection. In: BIOSENSORS &  
BIOELECTRONICS, 118, p. 58-65.

DOI: 10.1016/j.bios.2018.07.032

Handle: <http://hdl.handle.net/1942/27697>

1 **Article type: Full Paper**

2

3 ***Micro-Patterned Molecularly Imprinted Polymer Structures on***  
4 ***Functionalized Diamond-Coated Substrates for Testosterone Detection***

5

6 *Evelien Kellens<sup>a§</sup>, Hannelore Bové<sup>a§</sup>, Thijs Vandenryt<sup>a</sup>, Jeroen Lambrechts<sup>a</sup>, Jolien Dekens<sup>a</sup>,*  
7 *Sien Drijkoningen<sup>a,b</sup>, Jan D'Haen<sup>a,b</sup>, Ward De Ceuninck<sup>a,b</sup>, Ronald Thoelen<sup>a,b</sup>, Tanja*  
8 *Junkers<sup>a,1</sup>, Ken Haenen<sup>a,b</sup> and Anitha Ethirajan<sup>a,b\*</sup>*

9

10 <sup>§</sup> Both authors contributed equally to this work

11 \* Corresponding author: anitha.ethirajan@uhasselt.be

12

13 <sup>a</sup> Institute for Materials Research (IMO), Hasselt University, Wetenschapspark 1 and  
14 Agoralaan D, 3590 Diepenbeek, Belgium

15 <sup>b</sup> IMOMECE, IMEC vzw, Wetenschapspark 1, 3590 Diepenbeek, Belgium

16

17

18

19

20

21

22

23

24

25

26

27

28

29

30

31

32 <sup>1</sup> Present address: School of Chemistry, 19 Rainforest Walk, Monash University Clayton,  
33 VIC 3800, Australia

34 Abstract

35 Molecularly imprinted polymers (MIPs) can selectively bind target molecules and can  
36 therefore be advantageously used as a low-cost and robust alternative to replace fragile and  
37 expensive natural receptors. Yet, one major challenge in using MIPs for sensor development  
38 is the lack of simple and cost-effective techniques that allow firm fixation as well as  
39 controllable and consistent receptor material distribution on the sensor substrate. In this work,  
40 a convenient method is presented wherein microfluidic systems in conjunction with in situ  
41 photo-polymerization on functionalized diamond substrates are used. This novel strategy is  
42 simple, efficient, low-cost and less time consuming. Moreover, the approach ensures a tunable  
43 and consistent MIP material amount and distribution between different sensor substrates and  
44 thus a controllable active sensing surface. The obtained patterned MIP structures are  
45 successfully tested as a selective sensor platform to detect physiological concentrations of the  
46 hormone disruptor testosterone in buffer, urine and saliva using electrochemical impedance  
47 spectroscopy. The highest added testosterone concentration (500 nM) in buffer resulted in an  
48 impedance signal of  $10.03 \pm 0.19$  % and the lowest concentration (0.5 nM) led to a  
49 measurable signal of  $1.8 \pm 0.15$  % for the MIPs. With a detection limit of 0.5 nM, the MIP  
50 signals exhibited good linearity between 0.5 nM to 20 nM concentration range. Apart from the  
51 excellent and selective recognition offered by these MIP structures, they are also stable during  
52 and after the dynamic sensor measurements. Additionally, the MIPs can be easily regenerated  
53 by a simple washing procedure and are successfully tested for their reusability.

54 **Keywords:** microfluidics, molecularly imprinted polymers, biosensors and body fluids

## 55 1 Introduction

56 The demand for the detection and quantification of molecules in the fields of  
57 molecular screening, clinical diagnostics, and food- and environmental analysis is growing  
58 fast. Often, target molecule quantification in samples is performed in laboratories using  
59 analysis techniques such as immuno-assays, gas and liquid chromatography (or others), which  
60 are time consuming, laborious, costly and require stringent conditions and specialized  
61 personnel (Fitzgerald et al. 2010; Vera et al. 2011; Wang et al. 2014; Wild 2013). Therefore,  
62 interest in the development of cheaper, reusable, faster and more user-friendly sensors is  
63 increasing. Typically, recognition elements that are capable of binding target molecules are  
64 immobilized on a signal transducer substrate in these sensors. The binding events can be  
65 translated *via* electronic or optical read-out techniques into a concentration-dependent signal  
66 (Chen et al. 2016; Liu et al. 2018; Yang et al. 2018a). Biological macromolecules such as  
67 antibodies, enzymes, and cells are commonly used as recognition elements since they possess  
68 highly fine-tuned and effective molecular recognition (Eersels et al. 2013; Gooding 2002; Liss  
69 et al. 2002; Wang 2001). However, typically these natural receptors are on the one hand  
70 costly and laborious to obtain, and on the other hand they exhibit physical and chemical  
71 instability as well as insufficient sensitivity in non-physiological environments (Ruigrok et al.  
72 2011). A compelling alternative is the use of so-called synthetic biomimetic receptors, which  
73 are highly stable and cost-effective. In this regard, the use of molecularly imprinted polymers  
74 (MIPs) has tremendous potential to be used as artificial receptors for biosensing applications  
75 (Piletsky et al. 2001; Sellergren 2000; Whitcombe and Vulfson 2001). In general, MIPs are  
76 obtained when the target/template molecule is present in the matrix during polymerization.  
77 The functional groups of the monomer are arranged around the template molecule through  
78 non-covalent or covalent interactions. After polymerization, the subsequent removal of the  
79 template leaves nano-cavities (**Figure 1A**). These cavities are complementary to the template  
80 in terms of size, shape, and arrangement of the functional groups, allowing these polymer

81 imprints to rebind the target molecule with high affinity and specificity (Peeters et al. 2012).  
82 In contrast with natural receptors, these artificial receptors allow for a long shelf-time storage  
83 as well as chemical and physical robustness, even in extreme pH-environments (Piletsky et al.  
84 2001; Sellergren and Allender 2005).

85 The geometries of MIPs can be chosen depending on the requirements of the  
86 application. For sensor applications, MIPs have been used in the form of *ex situ* prepared  
87 particles which were subsequently immobilized on the sensor substrate (Kamra et al. 2015;  
88 Peeters et al. 2013; Wackers et al. 2014) but also in the form of films or structures which are  
89 directly in situ polymerized and grafted on the sensor substrate (Chen et al. 2015; Fuchs et al.  
90 2013). Recently, simultaneous wet phase inversion and imprinting was used to obtain MIP  
91 films on electrode surfaces, where the sensor performance as a function of the film thickness  
92 was studied (Yang et al. 2018b). Frequently used sensor read-out techniques, which quantify  
93 the binding between the target molecule and MIP based sensing electrodes, include  
94 impedance spectroscopy (Betatache et al. 2014), quartz crystal microbalance (Reimhult et al.  
95 2008) and surface plasmon resonance (Tan et al. 2015).

96 MIPs in the form of *ex situ* prepared particles are very interesting for sensor applications  
97 due to their high and controllable active sensing surface. Bulk polymerization with subsequent  
98 grinding is an established and widely used method as it is a fast and simple method to produce  
99 MIPs. As the bulk monoliths after mechanical grinding results in micron-sized particles with  
100 irregular shapes and sizes (Alexander et al. 2006; Svenson and Nicholls 2001), the  
101 applicability of these particles on sensor substrates is of concern. It is of most importance that  
102 the detection of a target molecule in a sample is reliable and consistent. Therefore, all  
103 inhomogeneities between different transducer substrates need to be reduced to a minimum. To  
104 obtain more control over the shape, particle size and surface area of the MIPs, colloidal MIP  
105 synthesis methods such as precipitation (Yang et al. 2010), suspension (Pérez-Moral and  
106 Mayes 2004), and emulsion (Vaihinger et al. 2002) techniques are compelling alternatives.

107 Issues which still need to be overcome are stable MIP attachment to the substrate (even in  
108 dynamic conditions) and consistency in amount and distribution of the polymer in and  
109 between different sensor substrates. Therefore, there has been a tremendous focus on  
110 techniques that allow to create stable and reliable sensing substrates in a reproducible way.  
111 MIP particles have been previously deposited using methods such as stamping, screen-  
112 printing, drop casting and spin coating (Chianella et al. 2003; Lavine et al. 2007; Wackers et  
113 al. 2014). In general, reliable MIP attachment, a consistent material amount and distribution  
114 on the substrate are important issues for sensor measurements. However, with these  
115 deposition techniques one or a combination of these issues still exist. With stamping  
116 procedures, substrates with an adhesive layer are used and the particles are pressed on to the  
117 adhesive polymer using a stamp. As the MIP is partially embedded into the adhesive layer,  
118 not the entire MIP particle is available for recognition purposes. In addition, partial  
119 embedding might likely cause problems if the particles come loose during the measurement.  
120 Moreover, if bulk MIP particles in the form of dried powder are stamped it is difficult to  
121 control the material amount and distribution on the adhesive layer. In case of screen printing,  
122 additional additives are needed which might block the MIP surface or interfere with the  
123 recognition ability of the MIP, depending on the choice of the additives used. Furthermore,  
124 when drop casting or spin coating approaches are employed, dispersions of particles in  
125 suitable solvents without aggregates are needed. Additionally, the dilution of the dispersion  
126 has to be optimal in order to have a good coverage on the substrate without aggregate  
127 formation. It is also crucial that the coated MIP particles on the substrate need to be firmly  
128 attached to the substrate in order to avoid problems during the sensor measurements. In this  
129 regard, particles have been immobilized on the biosensor substrate through linker molecules  
130 or by the use of an aforementioned adhesive polymer layer (Alenus et al. 2012; Kamra et al.  
131 2015; Peeters et al. 2012). Although these immobilization methods have proven their  
132 applicability, a stable coupling between the MIP particle and the substrate which is strong

133 enough to endure the dynamic sensor measurement conditions and ensure sensor regeneration  
134 for reusability remains challenging. In addition, many problems are still existing to find a  
135 technique that allows control over the MIP particle amount and distribution on the sensor  
136 substrate. Alternatively, homogeneous MIP films are also deposited on the substrates.  
137 However, depending on the thickness of the film, the removal of the template molecules  
138 might pose a problem due to the reduced surface area.

139 A major advance in the field was the direct *in situ* coupling and patterning of MIPs on the  
140 sensor surface. In this way, identical amounts and geometries of imprinted polymer can be  
141 achieved to act as molecular recognition layer. Previously, photolithographic methods  
142 (Acikgoz et al. 2011; Boysen et al. 2014) and advanced fabrication techniques such as  
143 scanning-beam, projection, and interference (holography) photography (Fuchs et al. 2013;  
144 Gates et al. 2004; Linares et al. 2011) have been reported. Also, non-optical based approaches  
145 including electrodeposition (Tretjakov et al. 2016), self-assembly (Apodaca et al. 2011), and  
146 microfluidic molds (Choi 2014) or stencils (Ayela et al. 2014) have been used. However,  
147 major problems associated with in situ patterning techniques are multi-step and time-  
148 consuming procedures and the use of expensive equipment. Therefore, it is highly desired to  
149 have a low-cost and time-efficient method which ensures on the one hand that every time  
150 identical amounts of pre-polymerization precursor mixture are polymerized in identical  
151 geometries with a high active sensing surface, and on the other hand an extremely firm  
152 attachment of the latter on the sensor substrate. The high surface area allows for reducing the  
153 total washing time to remove the template molecules to a minimum, which leads to a faster  
154 regeneration of the substrate. The bond between the MIP material and the sensor substrate  
155 should be strong enough so that no polymer detaches during the sensor measurements. This  
156 ensures the reliability of the sensor detection results and allows for successful reusability of  
157 the sensor substrate.

158 In this work, we report a simple and elegant fabrication of patterned MIP structures with  
159 geometries defined by the microfluidic stamp and the reliable attachment to the diamond  
160 electrode surface for the convenient detection of physiological concentrations of testosterone  
161 in samples comprising of real biological fluids using an impedimetric set-up under dynamic  
162 flow conditions (**Figure 1B**). Electrochemical impedance spectroscopy (EIS) was used as an  
163 electronic read out technique as it is sensitive, simple to use, inexpensive, fast, offers  
164 miniaturization possibilities, and integration with other techniques if needed. A boron-doped  
165 bio-inert nano-crystalline diamond (NCD) layer deposited on a highly doped silicon wafer  
166 was used as a substrate/electrode material. The conductive NCD was used as sensor interface  
167 for biological applications because of the materials' unique properties, namely the large  
168 electrochemical potential window, chemical inertness, physicochemical stability and  
169 biocompatibility (Bakowicz-Mitura et al. 2007; Grieten et al. 2011; Rubio-Retama et al. 2006;  
170 Vermeeren et al. 2011; Wenmackers et al. 2009). Due to its poor chemical stability, bare  
171 silicon substrates are prone to the formation of a silicon oxide layer, which would cause a drift  
172 in the impedance signal due to increasing capacitive effects. Various approaches to  
173 immobilize (bio-) molecules on diamond thin films have already been investigated (Hartl et al.  
174 2004; Hernando et al. 2007; Yang et al. 2002) and have also been successfully tested further  
175 for impedimetric sensing (van Grinsven et al. 2011). In this work, molecularly imprinted  
176 polymer structures were immobilized on diamond substrates by means of a simple and  
177 efficient carbon coating step combined with microfluidic molds. This approach allows for  
178 obtaining MIP structures with a controlled morphology. Jordan and co-workers have  
179 successfully demonstrated carbon templating on diamond substrates for grafting polymer  
180 chains and biofunctionalization (Hutter et al. 2011; Steenackers et al. 2009). Although a high  
181 spatial resolution and a small size range can be achieved, the drawback of the previously used  
182 method for carbon templating is that for every sensor substrate electron beam (e-beam)  
183 lithography needs to be performed, which is expensive and laborious. Therefore, in here the

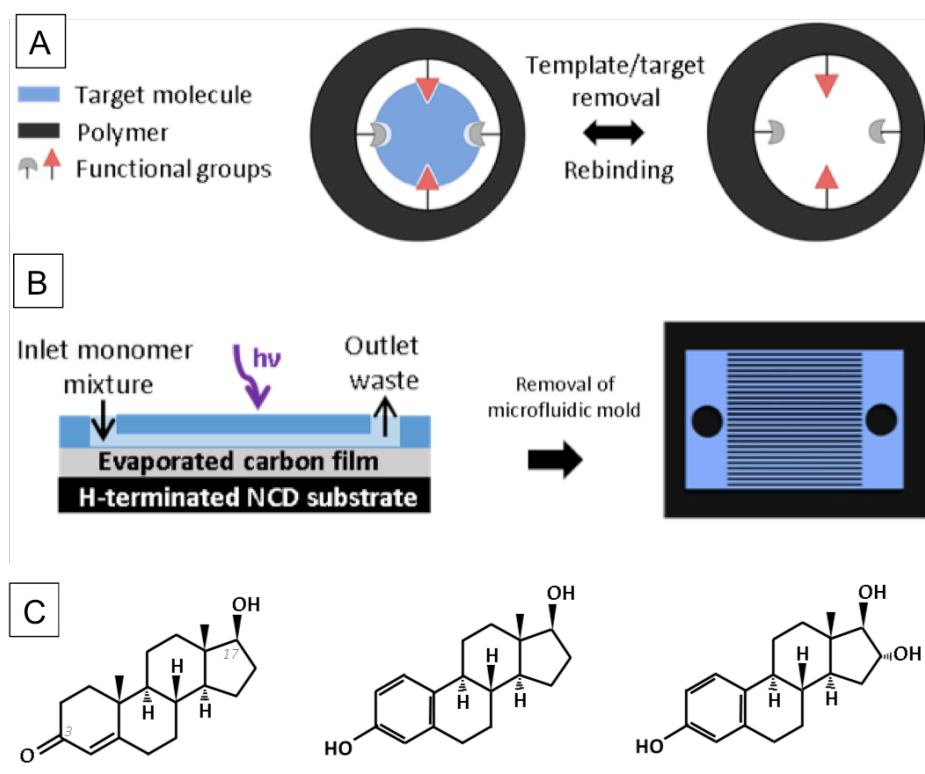


184 focus is laid on reducing the multi-step and time consuming synthesis procedures by using a  
185 simple and fast carbon coating step to deposit a stable thin layer (20 nm) of amorphous  
186 carbonaceous material over the whole transducer interface. The reactive bonds of the  
187 amorphous carbon allow ultraviolet (UV)-induced photografting and covalent attachment of  
188 polymer structures across the entire sensor surface. To structure the polymer into patterned  
189 MIP structures with effective transducer surface coverage and defined dimensions, the  
190 monomer-target molecule precursor mixture is deposited on the substrate by using a patterned  
191 elastic polydimethylsiloxane (PDMS) based microfluidic flow cell. To obtain this PDMS flow  
192 cell, first a master structure is created using e-beam lithography. Subsequently, from this  
193 master structure, numerous PDMS molds can be obtained using the master as a cast. As a  
194 proof of concept, MIP structures for testosterone detection were targeted. Testosterone is a  
195 steroid hormone disruptor and concentrations deviating from the physiological concentrations  
196 are associated with several health conditions (Thieme and Hemmersbach 2009), like breast  
197 cancer in women (Cauley et al. 1999) as well as prostate and lung cancer in men (Hyde et al.  
198 2012). A bi-functional crosslinking monomer – N,O-bismethacryloyl ethanolamine (NOBE)  
199 (LeJeune and Spivak 2007) – was used as we have shown previously that NOBE is a very  
200 suitable monomer for the non-covalent imprinting of testosterone (Kellens et al. 2016). It is  
201 worth to note that by using a bi-functional monomer the need for additional functional  
202 monomers and empirical optimization of the relative ratios in the formulation is eliminated.  
203 After the photografting and in situ polymerization of the monomer-target molecule precursor  
204 mix, the template molecules were removed from the imprints by washing steps. The emptied  
205 cavities are then available for rebinding of the template molecule with high affinity and  
206 specificity.

207         The use of microfluidic systems in combination with MIPs is already described in  
208 literature (Birnbaumer et al. 2009; Choi 2014; Weng et al. 2007). However, the combination  
209 of micropatterned MIP structures and reliable immobilization on an electrochemically inert

210 NCD sensor substrate using a coordinated sequence of simple surface treatment steps  
 211 (hydrogen termination followed by thin carbon layer deposition) for selective impedimetric  
 212 sensing of target molecules has to the best of our knowledge not been reported yet in literature.  
 213 For every sensor measurement, a non-imprinted polymer (NIP) structure with identical  
 214 geometries was used. This negative control was synthesized and handled in the same way as  
 215 the MIP but in the absence of the template molecules during polymerization. To test the  
 216 selectivity of the MIP structures for the target molecule, the binding characteristics towards  
 217 molecules that are structurally similar to testosterone, such as estriol and  $\beta$ -estradiol, are  
 218 tested (**Figure 1C**).

219



220  
 221 **Figure 1:** (A) Scheme showing the principle to obtain molecularly imprinted polymers. (B)  
 222 Schematic representation of the method to reliably obtain microstructured MIPs using  
 223 microfluidics and in situ photo-polymerization. (C) Chemical structures of the target molecule  
 224 testosterone and its structural analogues  $\beta$ -estradiol and estriol (from left to right).

225

## 226 2 **Materials and methods**

### 227 2.1 *Materials*

228 All chemicals and materials were purchased from VWR or Sigma-Aldrich unless stated  
229 otherwise. Column chromatography was conducted on silicon dioxide (EcoChrom) and 80 g  
230 silica cartridges (Grace Davison Discovery Sciences) using a Büchi automatic column  
231 chromatography device. For the fabrication of the microfluidic PDMS stamps, the silicone  
232 Sylgard elastomer kit 184 was purchased from Dow Corning Corp, and a 1 mm disposable  
233 biopsy punch (Miltex) and Teflon tubes with an outer diameter of 1.17 mm (Alpha Wire)  
234 were used. Testosterone, estriol and  $\beta$ -estradiol were purchased from Fluka Analytical.  
235 Phosphate buffered saline packs were obtained from Thermo Scientific.

### 236 2.2 *Synthesis of N,O-bismethacryloyl ethanolamine (NOBE)*

237 For the synthesis of NOBE, a previously reported procedure was followed (Kellens et al.  
238 2016). NOBE was synthesized by mixing 0.450 mol ethanolamine and 0.900 mol  
239 triethylamine in dry dimethylformamide with dropwise addition of 1.125 mol methacryloyl  
240 chloride under nitrogen at 0 °C. The mixture was stirred for 24 h at 40 °C and afterwards  
241 diluted with ethyl acetate. The formed ammonia salts were removed by filtration. All water-  
242 soluble contents were extracted by washing with saturated sodium bicarbonate, saturated  
243 ammonium chloride, water and saturated sodium chloride aqueous solutions, respectively.  
244 The crude product was dried with magnesium sulfate and passed over a basic alumina column  
245 to remove residual acids. For the final purification, the product was passed over a silica  
246 column using ethyl acetate/petroleum spirit (5/95 ratio) as mobile phase. The monomer yields  
247 before and after purification are 85 % and 35 % respectively. Since the monomer is prone to  
248 self-polymerization, a significant amount of material is lost during purification. For nuclear  
249 magnetic resonance (NMR) data we refer to previously reported results (Kellens et al. 2016).

250

251

252 **2.3 *Design and Fabrication of Microfluidic Mold***

253 **2.3.1 *Design and Fabrication of Master Mold***

254 Prior to spin coating, 1 cm x 1 cm silicon substrates (L14016, Siegert Wafer GmbH) were  
255 thoroughly cleaned and dehydrated by heating them for 5 min at 150 °C. The negative  
256 photoresist SU-8 2025 (Micro Resist Technology GmbH) was diluted by cyclopentanone  
257 from a solid-content of 68.6 % to 44.4 %. These solutions were spin coated following  
258 manufacturer's specifications and cured for 2 min at 95 °C, resulting in a thick layer of  
259 approximately 4.5 µm. The desired pattern of the MIP structures, with specified widths and  
260 heights, were designed with the DesignCad It 2000 software tool. E-beam lithography was  
261 performed with a NPGS system (JC Nability Lithography Systems) mounted on a FEG-SEM  
262 (FEI Quanta 200F). The e-beam line-exposure was set at 0.12 nC/cm with an acceleration  
263 voltage of 30 kV. After exposure, the SU-8 layers were baked again for 3 min at 110 °C. The  
264 substrates were developed with SU-8 developer and rinsed with 2-propanol. The master mold  
265 was additionally subjected to a hard-baking step for 2 h at 150 °C to release stress from the  
266 resulting SU-8 microstructures and to achieve optimal mechanical stability and durability.  
267 The mold can then be reused dozens of times without deteriorating performance.

268 **2.3.2 *Design and Fabrication of Microfluidic Stamp***

269 A cast from the master mold was made in PDMS. The base polymer and curing agent were  
270 mixed thoroughly in a 10:1 weight-ratio in a disposable recipient. The introduced air from  
271 mixing was removed at an absolute pressure of 0.55 bar for at least 30 min. Next, the uncured  
272 PDMS was poured over the mold and subsequently baked in an oven for 3 h at 60 °C under  
273 normal atmosphere. The resulting PDMS cast of 2.5 mm high was cut out with a scalpel and  
274 peeled off from the mold. The inlet and outlet (hereinafter referred to as connection blocks)  
275 were punched using a 1 mm biopsy punch and the excess of cured PDMS was removed.

276

277

278 *2.3.3 Surface Treatment of NCD Substrates*

279 Highly doped silicon substrates (resistivity 10 – 20 k $\Omega$ , p-type doping, 10 mm x 10 mm x  
280 0.525 mm) overgrown with a < 200 nm NCD layer ( $[\text{CH}_4]/[\text{H}_2] = 4\%$ ,  $[\text{TMB}]/[\text{CH}_4] = 4800$   
281 ppm) were cleaned by wet etching for 30 min in an oxidizing mixture of boiling potassium  
282 nitrate and sulfuric acid (1:10 ratio), followed by washing in an ultrasonic bath with heated  
283 ultrapure water. Next, the substrates were thoroughly rinsed with ultrapure water and dried  
284 using nitrogen gas. Hydrogenation of the substrates was performed using an ASTeX® reactor  
285 equipped with a 2.45 GHz microwave generator: 2 min at 3500 W, 30 Torr, 500 sccm H<sub>2</sub> and  
286 5 min at 2500 W, 15 Torr, 500 sccm H<sub>2</sub>. The substrates were cooled in H<sub>2</sub> atmosphere (500  
287 sccm) for 40 min. Subsequently, a 20 nm thick carbon layer was deposited at 40 amperes onto  
288 the H-terminated substrates (Leica EM ACE600, carbon thread evaporation).

289 *2.3.4 Fabrication of Patterned MIP Structures*

290 The formulation used for the fabrication of the MIP structures was achieved by adapting a  
291 protocol that was previously published (Kellens et al. 2016), where the affinity and selectivity  
292 of the used monomer/target combination and ratio has been studied. The formulation was  
293 however optimized to achieve a mixture that can flow through the channels. The tested  
294 variations are shown in Table S1. The optimal mixture used comprised of 0.507 mmol NOBE,  
295 0.012 mmol 2,2-dimethoxy-2-phenylacetophenone, 1.088 mmol chloroform and 0.087 mmol  
296 testosterone.

297 The microfluidic stamp was placed onto the freshly carbon coated NCD substrate and  
298 Teflon tubes were connected to the inlet and outlet of the stamp. The polymerizable mixture  
299 was pumped via the inlet through the microfluidic channels until they were all filled. Next, the  
300 tubes were removed and the substrate, with filled microfluidic channels, was placed under  
301 UV-light (Lawtronics ME5E UV-lamps, 254 nm, 265 mW/cm<sup>2</sup>). The UV-transmittance of  
302 PDMS at 254 nm ranges between 40 and 60 % (**Figure S1** in the supplementary information

303 (SI). Polymerization was done for 20 h in a glovebox under nitrogen environment. After  
304 polymerization, the stamp was removed from the substrate.

305 The target molecules were removed from the MIP structures by gently shaking the  
306 substrate in a mixture of 1:1 ethanol (EtOH)/ultrapure water (7.5 h, 5x solvent change), a  
307 mixture of 1:19 acetic acid/methanol (4 h, 2x solvent change), and a mixture of  
308 ethanol/ultrapure water (1 h, 4x solvent change). Non-imprinted polymer structures were  
309 synthesized in the absence of the target molecule and washed following the same procedure as  
310 for the MIP structures.

#### 311 **2.4 Characterization of the patterned polymer structures**

312 The integrity of the structures was characterized using an Axiovert 40 MAT optical  
313 microscope (Zeiss) equipped with a digital camera and by using the Axiovision AC software.  
314 The integrity and geometry of the structures were studied using a scanning electron  
315 microscope (SEM, FEI Quanta 200F) operating at an accelerating voltage around 20 kV. The  
316 morphology and height of the structures were measured employing the DektakXT  
317 profilometer (Bruker).

#### 318 **2.5 Electrochemical Impedance Spectroscopy (EIS)**

319 The electrochemical testing of the patterned MIP/NIP structures as sensor platform was  
320 performed using impedance spectroscopy. The measurements were executed using a custom  
321 designed differential impedance sensor-cell set-up (**Figure 3A**), which can measure both MIP  
322 and NIP substrates simultaneously, thereby eliminating the influence of the surroundings  
323 (such as temperature fluctuations) and sample variations (such as different biological residue  
324 content).

325 The flow-through cell has an internal volume of 300  $\mu$ L and is made of polymethyl  
326 methacrylate. All measurements were temperature controlled using a proportional integral  
327 derivative controller (P = 5, I = 8, D = 0). The MIP- and NIP-coated electrodes were installed  
328 symmetrically with respect to a gold wire serving as a common counter electrode. The contact

329 area of each electrode with the liquid was defined by O-rings (28 mm<sup>2</sup>), and the distance from  
330 the sensing substrates to the counter electrode was 1.7 mm. Two other (ground) electrodes are  
331 present on the copper block of each substrate. The impedance signals were measured in a  
332 frequency range of 100 Hz to 100 kHz with 10 frequencies per decade and a scanning speed  
333 of 5.69 s per sweep. The amplitude of the alternating current voltage was fixed to 10 mV  
334 under open circuit conditions. Silver paste was used to improve the contact between the  
335 transducer substrate and the copper blocks.

## 336 **2.6 Electrochemical Testing of MIP/NIP structures as Sensor Platform**

337 The binding behavior of the MIP and NIP structures for testosterone was tested using EIS at  
338 the physiological pH (7.4) and temperature (37 °C). Testosterone solutions were prepared  
339 using ethanol/aqueous media mixtures as the former had limited solubility in water. For these  
340 experiments, a mix of ethanol and 1x phosphate buffered saline (PBS) solution, filtered urine  
341 or saliva (in a 20/80 wt. % ratio, passed through Chromafil filters for polar media, pore size 1  
342 and 5 µm) was spiked with testosterone to obtain the following target molecule  
343 concentrations: 0.5, 2, 8, 20, 50, 100, 300 and 500 nM. Subsequently, the sensor substrates  
344 were integrated in the differential sensor set-up and the impedance signal was allowed to  
345 stabilize in the ethanol/buffer, urine or saliva solution containing no target or analogues  
346 molecules (blank sample). After stabilization, 1 mL of the spiked samples was added, from  
347 low to high concentration with 15 minutes intervals. To obtain the dose-response graphs, the  
348 mean impedance value of the last 35 data points obtained after administration of a certain  
349 concentration ( $Z(t)$ ) was normalized with the initial impedance stabilization value (blank  
350 sample,  $Z(0)$ ). The obtained value was plotted against that specific testosterone concentration.  
351 Informed signed consent was obtained from the healthy volunteer who donated urine and  
352 saliva. To test the cross-selectivity, impedance measurements were conducted for the  
353 structural analogues  $\beta$ -estradiol and estriol using the following concentrations: 0.5, 2, 8, 20,  
354 50 and 100 nM.

### 355 3 Results and Discussion

356 In this work, a patterned MIP structure immobilized on a sensor substrate was realized  
357 by combining simple and efficient functionalization of diamond substrates using amorphous  
358 carbon coating and patterned microfluidic molds. The bi-functional monomer NOBE was  
359 obtained using a previously reported synthesis method (Kellens et al. 2016; LeJeune and  
360 Spivak 2007), and testosterone was used as template molecule. The resulting MIP structures  
361 were characterized by optical light microscopy, Dektak profilometry and SEM. For the proof-  
362 of-concept, the sensor performance was tested using EIS in buffer, urine and saliva spiked  
363 with testosterone. The highly stable bonds between the polymer structures and the substrate  
364 allowed for successful regeneration of the sensor substrates. The selectivity of the sensor was  
365 tested using testosterone structural analogues, namely estriol and  $\beta$ -estradiol.

366

#### 367 3.1 Fabrication of patterned MIP structures

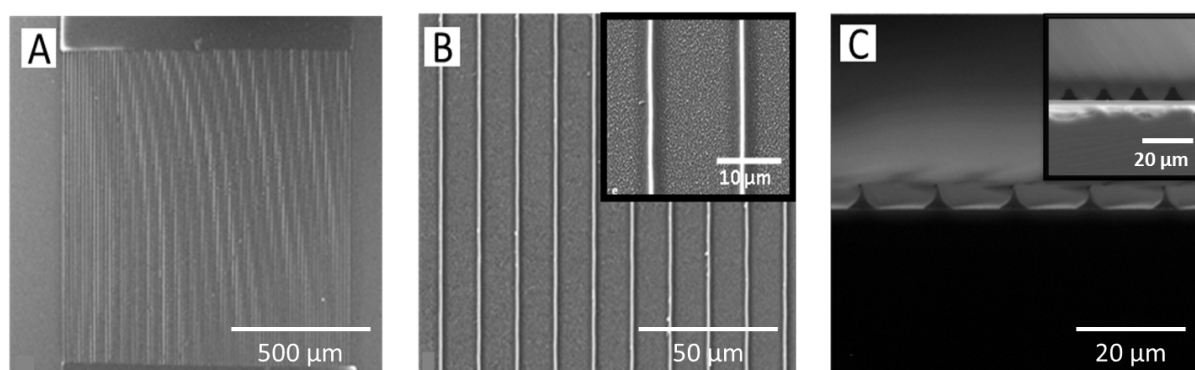
368 The new design strategy for the immobilization of MIP structures overcomes the  
369 aforementioned disadvantages related to *ex situ* prepared MIP particles and other *in situ*  
370 strategies. It includes the direct synthesis of micron-sized MIP structures onto a hydrogen-  
371 terminated and carbon-coated (20 nm thick carbon film) nano-crystalline diamond layer on  
372 top of highly doped silicon transducer substrates by UV-induced photo-polymerization of  
373 vinyl groups, as well as photografting to the carbon layer (**Figure 2**). This process involves  
374 few simple sequential steps: initially, carbonaceous material is deposited onto the hydrogen-  
375 terminated surface of the diamond transducer element to ensure the subsequent attachment of  
376 the MIP structures to the substrate. The role of carbon functionalization is crucial as hydrogen  
377 termination of NCD substrates alone for photografting was not sufficient to yield a stable  
378 immobilization of the polymer layer (see further text). The integrity of these MIP structures  
379 on top of the NCD substrates was checked by Dektak profilometry (SI, **Figure S2 and Figure**  
380 **S3**) and optical microscopy (SI, **Figure S4**). From these analyses, no structural differences



381 can be observed between MIP and NIP structures. Even after several washing steps the  
382 structures were still intact, thereby reflecting the stability of the MIP structures on the  
383 substrate. On the contrary, in case of hydrogen termination of NCD substrates without carbon  
384 functionalization, the polymerized structures did not survive the washing steps and were  
385 detached from the substrate. This control experiment clearly demonstrates the need for the  
386 carbon functionalization step prior to polymerization for a stable immobilization of the  
387 polymeric structures on the substrate.

388 Top view and cross-section images of these polymer structures were obtained using  
389 SEM (**Figure 2 A - C**). From the cross-section image it can be observed that the polymer  
390 structures have a shape resembling the PDMS stamp, however with a reduced dimension as a  
391 consequence of polymerization induced shrinkage.

392



393  
394 **Figure 2.** SEM images depicting polymer structures on NCD substrates: (A) Overview  
395 illustrating the patterned structure; (B) Top view of structures in higher magnification with the  
396 insert showing two lanes in focus, (C) Cross-section view of the polymer structures with the  
397 insert showing a cross section of the PDMS stamp.

398

### 399 **3.2 Impedimetric testing of patterned MIP structures as sensor platform in buffer** 400 **solution**

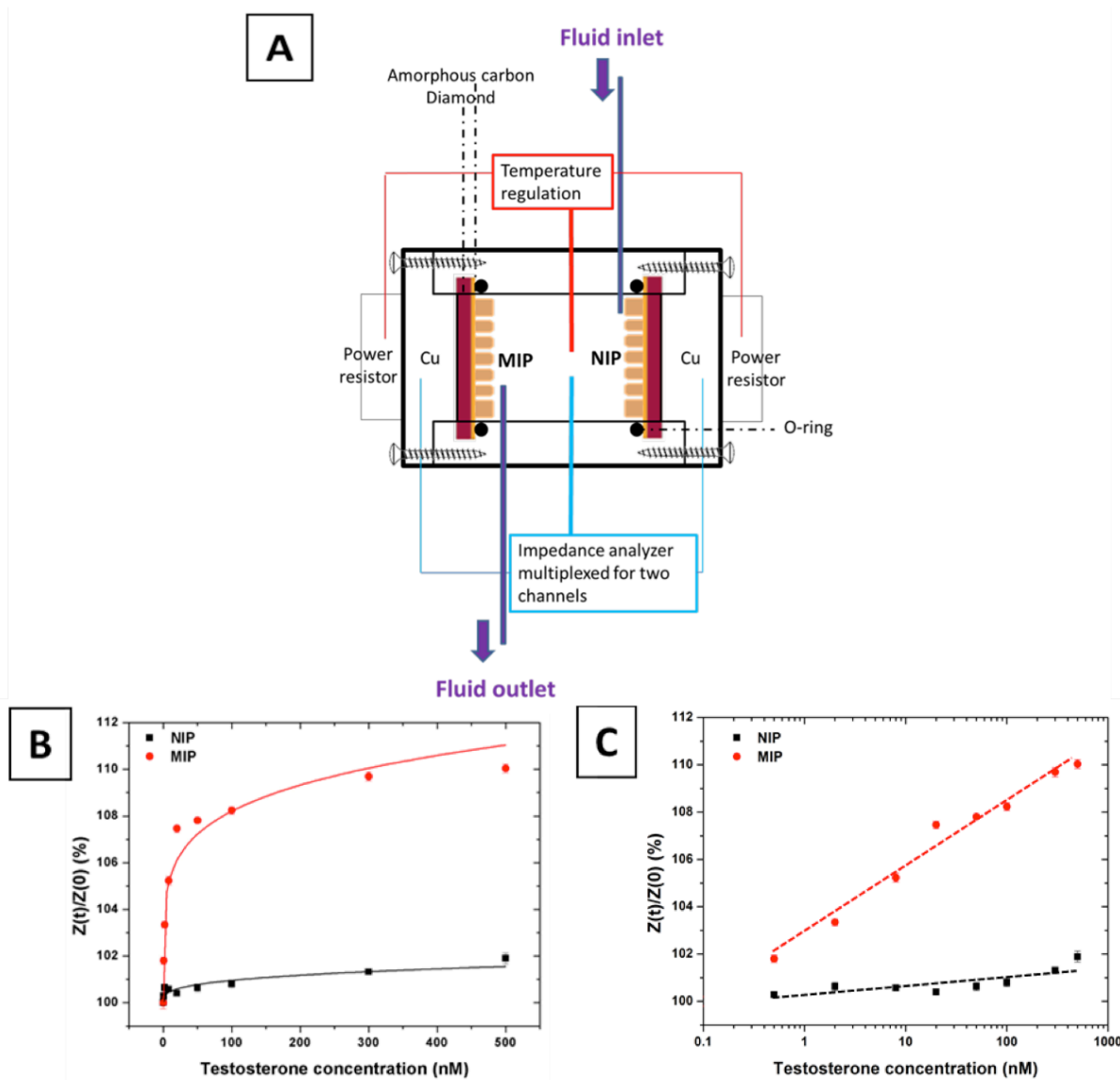
401 As proof-of-concept, the synthesized MIP sensor platform was tested by electronic  
402 sensing based on EIS. Both MIP and NIP structures have an identical surface coverage and  
403 polymer distribution as they were synthesized using identical PDMS stamps. Therefore, the  
404 precondition for differential measurements – having identical surface loadings – was  
405 complied.

406 For the detection using EIS, a custom designed differential set-up was used to measure  
407 the binding activity of the MIP and NIP in an identical environment (**Figure 3A**). The flow-  
408 through cell was filled with an ethanol/PBS solution (20/80 wt. %) at a pH of 7.4 to simulate a  
409 physiological acidity environment. After stabilization at the physiological temperature of  
410 37 °C, 1 mL of increasing known concentrations of testosterone ranging between 0.5 and 500  
411 nM was added stepwise with intervals of 15 minutes. All dose-response curves for  
412 testosterone detection in buffer solutions were determined at a frequency of 1,258 Hz. This  
413 frequency was chosen because it offered a good signal-to-noise ratio, which resulted in a very  
414 stable impedance signal with a small standard deviation of approximately 0.18 %.

415 The resulting dose-response curves are shown in **Figure 3**. The y-axis represents the  
416 normalized impedance change and the x-axis the concentration of administered testosterone.  
417 The graphs in **Figure 3** clearly demonstrate that a significant difference exists in sensor  
418 response between the MIP and NIP upon increasing target molecule concentration. The  
419 binding of testosterone to the polymer causes an increase in the complex resistance. The  
420 highest added testosterone concentration (500 nM) resulted in an increase of the impedance  
421 signal with  $10.03 \pm 0.19$  % for the MIP and  $1.89 \pm 0.23$  % for the NIP. Even the addition of  
422 the lowest testosterone concentration (0.5 nM) led to a measurable increase in the MIP signal  
423 of  $1.8 \pm 0.15$  %, which is clearly visible from the plot in the logarithmic scale (**Figure 3B**).  
424 This testosterone concentration is situated well within the physiological range of 0.5 – 60 nM  
425 (Jin et al. 2007; Taieb et al. 2003). The sensor response of the NIP was comparatively low,  
426 indicating only small amounts of aspecific binding of testosterone. The latter is in accordance

427 with our previous reported studies (Kellens et al. 2016). The increase in the occupation of the  
428 MIP binding sites by testosterone leads to a trend toward saturation for concentrations higher  
429 than 20 nM. The impedimetric response upon target binding was modeled using an equivalent  
430 circuit (SI, **Figure S5 and Table S2**). The change in the impedance signal is attributed to the  
431 change in the capacitance at the functionalized electrode interface due to the binding of the  
432 testosterone molecules to the MIP cavities. This observation is in accordance to the previous  
433 findings (Peeters et al. 2012) where it was described that the binding leads to the replacement  
434 of water molecules by the organic molecules (lower dielectric constant as compared to water).  
435 Additionally, the effective contact area between the electrode and electrolyte is also affected  
436 as more target molecules bind to MIP layer. In our case, as the substrate is a highly doped  
437 semiconductor, the electronic properties of the substrate with the MIP functional layer is also  
438 influenced by the target molecule binding, while the NIP substrate shows no characteristic  
439 change in its electronic properties.

440

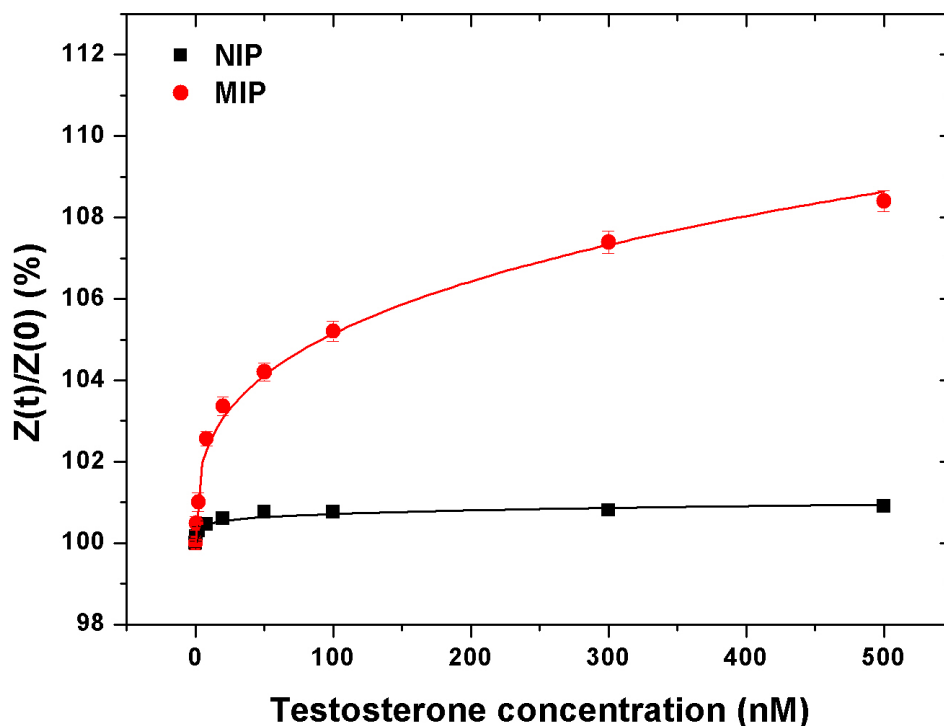


441  
 442 **Figure 3.** (A) Schematic representation of the differential impedimetric flow cell used for the  
 443 simultaneous measurements of MIP and NIP substrates; (B) EIS dose-response curves (fitted  
 444 non-linearly,  $R^2 = 0.91$  for MIP and  $0.87$  for NIP) of the MIP and NIP structures exposed to  
 445 increasing concentrations of testosterone in EtOH/PBS buffer solution; (C) Dose-response  
 446 curves identical to (B) but with the testosterone concentration plotted in logarithmic scale to  
 447 clearly illustrate the response at the lowest concentrations. The dotted lines serve as a guide to  
 448 the eye to give an indication about the linear behavior at these concentrations.  
 449

450 The obtained result clearly proves that by employing this simple fabrication technique,  
451 a sensor platform with well-defined MIP structures is achieved, resulting in sensitive and high  
452 performance measurements. In addition, as a proof of concept, the sensor substrate was tested  
453 for reusability by washing the bound testosterone molecules. As a proof for regeneration, the  
454 substrates that were used to construct **Figure 3** were washed subsequently for a second time  
455 with the same solvent mixtures (as explained in the experimental section) to remove bound  
456 testosterone from the polymers. The polymer structures remained intact after washing when  
457 observed with the optical microscope. A subsequent impedance sensor measurement was  
458 performed with these substrates and the resulting dose response curve is shown in **Figure 4**.

459 From **Figure 4** it can be seen that the MIP structures are still capable of binding a high  
460 amount of testosterone in comparison to the NIP structures, even after regeneration. When the  
461 highest concentration of testosterone is added (500 nM), the impedance signal increases by  
462  $(8.40 \pm 0.26)$  % for the MIP and  $(0.90 \pm 0.09)$  % for the NIP. However, these values are not  
463 as high as the values obtained from the previous sensor measurement. This effect can be due  
464 to incomplete testosterone removal after the second washing procedure, which can be  
465 improved by optimizing the washing protocol.

466



467

468 **Figure 4:** EIS dose-response curves (fitted non-linearly,  $R^2 = 0.93$  for NIP and  $0.99$  for MIP)

469 of the regenerated MIP and NIP substrates.

470

### 471 3.3 Selectivity testing of the sensor platform in buffer solution

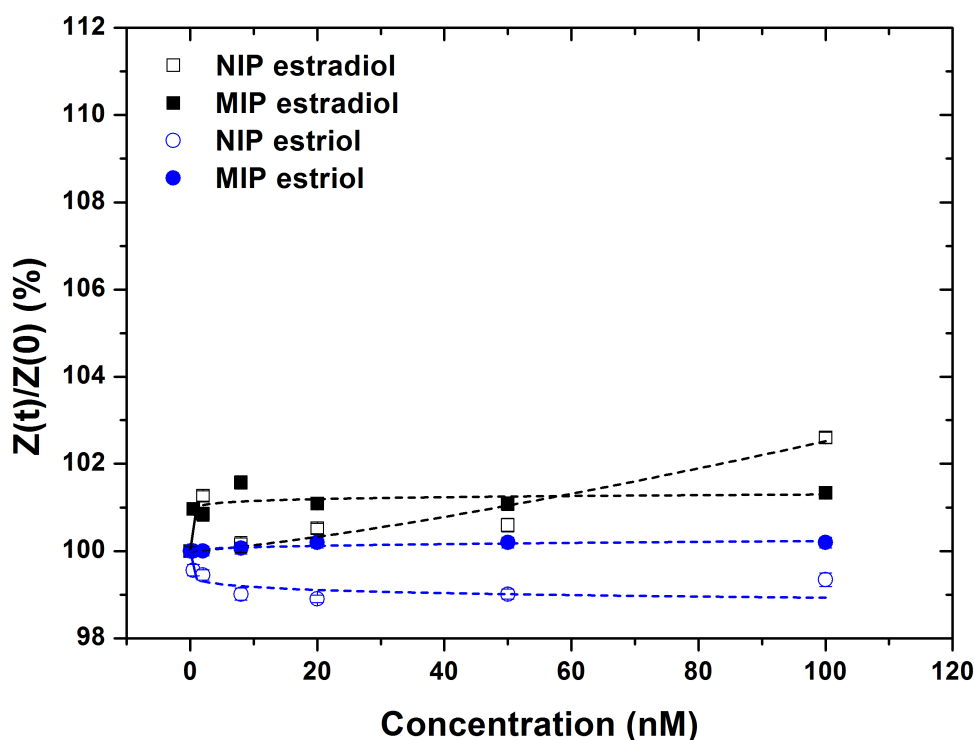
472 To test the selectivity of the MIP structures, sensor measurements were performed

473 wherein testosterone was replaced with structurally similar molecules. The obtained dose-

474 response data recorded at a frequency of 1,258 Hz for the MIP and NIP structures exposed to

475 increasing concentrations of estriol and  $\beta$ -estradiol are shown in **Figure 5**.

476



477  
 478 **Figure 5.** EIS dose-response curves of the MIP and NIP structures exposed to increasing  
 479 concentrations of estriol and  $\beta$ -estradiol in EtOH/PBS buffer solution. The dotted lines serve  
 480 as a guide to the eye to show the trend of the sensor response.

481  
 482 It can be clearly seen that  $\beta$ -estradiol shows some affinity to the MIP structures while  
 483 estriol shows no specific binding at all. A concentration of 100 nM resulted in an increase of  
 484 the MIP impedance signal with  $0.19 \pm 0.12$  % for estriol and  $2.6 \pm 0.12$  % for  $\beta$ -estradiol.  
 485 Both estriol and  $\beta$ -estradiol are different from testosterone since they both lack the methyl  
 486 group at the C-19 position and have a hydroxyl group at the C-3 position instead of a ketone.  
 487 Compared to  $\beta$ -estradiol, estriol shows the largest structural variation with testosterone  
 488 because of its excess hydroxyl group at the C-16 position, which provides steric hindrance  
 489 during the binding to the testosterone imprints. This explains the low or non-existing affinity  
 490 between the MIP and estriol.  $\beta$ -estradiol, which lacks the C-16 hydroxyl group, shows a small  
 491 affinity towards the obtained MIPs. However, this is still less pronounced in comparison with

492 the affinity for the template molecule testosterone. These findings are in agreement with our  
493 previous report and underpin the high selectivity of the MIPs obtained (Kellens et al. 2016).

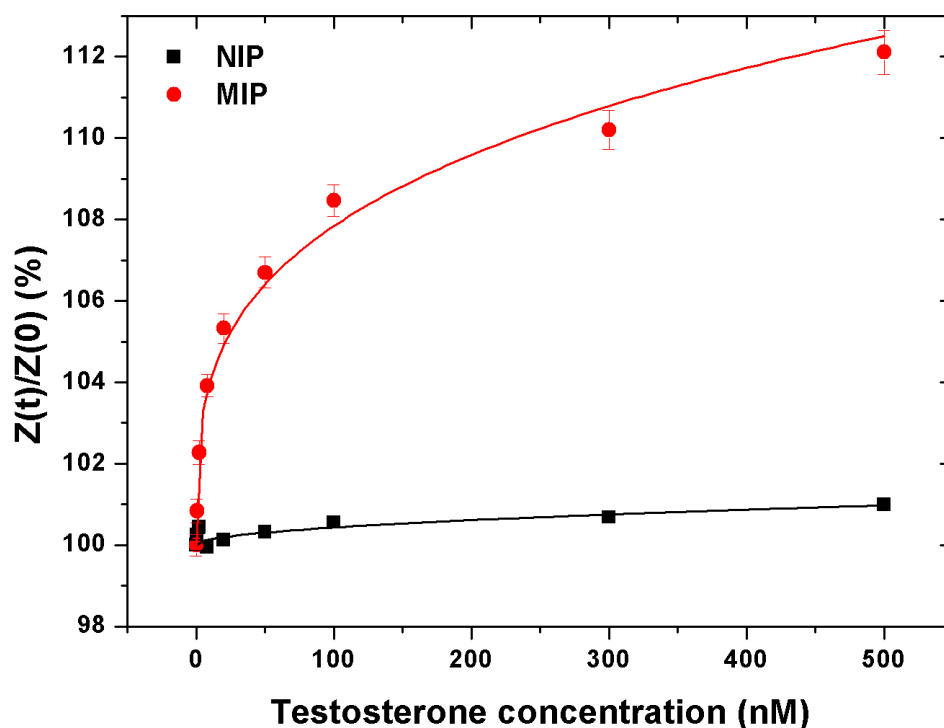
494

### 495 **3.4 Impedimetric testing of the sensor platform in body fluids**

496 After obtaining a selective response from the MIP structures in EtOH/PBS buffer  
497 solutions, the same experiments were performed with testosterone-spiked solutions where the  
498 PBS buffer was replaced with urine or saliva. These body fluids were obtained from a healthy  
499 volunteer and, as a preparation step, they were filtered in order to remove large structures (any  
500 residual cells and other large impurities). This way, the binding characteristics of the MIP and  
501 NIP structures can be analyzed in the presence of other molecules such as hormones, vitamins,  
502 proteins, etc., which are present in real patient samples that can potentially block the imprints.  
503 The results obtained with the EtOH/urine solution are shown in **Figure 6**. The optimal  
504 frequency – where the highest signal to noise ratio is observed – for the measurements was  
505 501 Hz due to the presence of proteins, hormones, or other potentially interfering substances  
506 in urine.

507





508  
 509 **Figure 6.** EIS dose-response curve (fitted non-linearly,  $R^2 = 0.80$  for NIP and  $0.98$  for MIP)  
 510 of the MIP and NIP structures exposed to increasing concentrations of testosterone in  
 511 EtOH/urine solution.

512  
 513 The maximum impedance increases of the NIP and MIP after adding a concentration  
 514 of 500 nM testosterone were  $(0.99 \pm 0.09)$  % and  $(12.11 \pm 0.53)$  % respectively. At lower  
 515 testosterone concentrations of 0.5 and 2 nM, the MIP structures gave a sensor response of  
 516  $(0.84 \pm 0.29)$  % and  $(2.27 \pm 0.29)$  %, respectively. This limit of detection is in accordance  
 517 with Batatache *et al.* where they combined MIP film detection with EIS read-out (Batatache *et*  
 518 *al.* 2014). These results show that even in complex samples, the MIP structure is still able to  
 519 detect testosterone in a specific way.

520 Also, in saliva-based samples the MIP structures were able to specifically bind  
 521 testosterone. The obtained results are shown in the supplementary information (**Figure S6**). In  
 522 saliva, the MIP sensor performance was lower compared to the one obtained in buffer and

523 urine; with a maximum impedance increase of  $(3.63 \pm 0.32)$  % at 500 nM testosterone. The  
524 impedance increase for the NIP at this testosterone concentration is  $(1.20 \pm 0.24)$  %. This  
525 effect can be explained by the fact that there are more proteins and other molecules present in  
526 saliva in comparison with buffer and urine which substantially block the testosterone imprints.  
527 However, this can in principle be circumvented by pretreating the saliva samples. Regardless,  
528 the MIP structures still show a better response than the control NIP structures.

529

530

## 531 **4 Conclusions**

532           Patterned microstructures of molecularly imprinted polymers on functionalized NCD  
533 substrates were created with testosterone as target molecule and NOBE as a bi-functional  
534 monomer. A master structure, which was obtained using e-beam lithography, was used to  
535 fabricate structured PDMS stamps. The latter were used to obtain patterned polymer  
536 structures that were covalently attached to the amorphous carbon coated diamond substrate.  
537 The obtained structures were characterized using optical microscopy, SEM and height  
538 profilometry. We could demonstrate that the structures remained intact on the substrate even  
539 after several washing steps. The affinity and selectivity of these sensor substrates for the  
540 target molecule testosterone were tested using EIS as a readout technique. The structured  
541 polymers were able to detect testosterone with a detection limit of 0.5 nM and showing  
542 saturation at concentrations above 20 nM. The ability to detect small concentrations with high  
543 specificity in buffer, urine and saliva samples shows the application potential of these  
544 structures. As a proof of concept, it was also shown that the polymer structures could be  
545 regenerated after a sensor measurement. This promising result opens new avenues toward  
546 reusable MIP based sensors.

547 It may be concluded that our approach offers a simple and cost-effective method to produce  
548 sensitive, high performant, reproducible and well-defined MIP based sensor platforms for the  
549 electronic detection of target molecules. The fabrication method offers design flexibility that  
550 can be used for tuning the dimensions and amount of MIP structures by opting for suitable  
551 master structures, which provide increased active sensing surfaces. The latter, in combination  
552 with a miniaturized measuring cell, can eventually lead to achievement of an even lower limit  
553 of detection. The microfabrication approach employing microfluidic molds can be extended to  
554 deposit multiple structures imprinted with different target molecules on the same substrate  
555 using independent stamps in order to realize applications that require multi-analyte sensing.

556 **Acknowledgements**

557 E.K. and H.B. contributed equally to this work. E.K. gratefully acknowledges the financial  
558 support by the Agency for Innovation by Science and Technology (IWT). H.B. is an FWO  
559 doctoral fellow. K.H. acknowledges the financial support provided by the Methusalem NANO  
560 network. The authors also thank additional financial support from UHasselt BOF funds. The  
561 authors gratefully acknowledge technical support by B. Ruttens, H. Pellaers, C. Willems, and  
562 J. Baccus.

563

564

565 **References**

- 566 Acikgoz, C., Hempenius, M.A., Huskens, J., Vancso, G.J., 2011. *Eur. Polym. J.* 47(11), 2033-  
567 2052.
- 568 Alenus, J., Galar, P., Ethirajan, A., Horemans, F., Weustenraed, A., Cleij, T.J., Wagner, P.,  
569 2012. *Phys. Status Solidi A* 209(5), 905-910.
- 570 Alexander, C., Andersson, H.S., Andersson, L.I., Ansell, R.J., Kirsch, N., Nicholls, I.A.,  
571 O'Mahony, J., Whitcombe, M.J., 2006. *J. Mol. Recognit.* 19(2), 106-180.
- 572 Apodaca, D.C., Pernites, R.B., Del Mundo, F.R., Advincula, R.C., 2011. *Langmuir* 27(11),  
573 6768-6779.
- 574 Ayela, C., Dubourg, G., Pellet, C., Haupt, K., 2014. *Adv. Mater.* 26(33), 5876-5879.
- 575 Bakowicz-Mitura, K., Bartosz, G., Mitura, S., 2007. *Surf. Coat. Technol.* 201(13), 6131-6135.
- 576 Betatache, A., Lagarde, F., Sanglar, C., Bonhommé, A., Léonard, D., Jaffrezic-Renault, N.,  
577 2014. *Sens. Trans. J.* 27, 92-99.
- 578 Birnbaumer, G.M., Lieberzeit, P.A., Richter, L., Schirhagl, R., Milnera, M., Dickert, F.L.,  
579 Bailey, A., Ertl, P., 2009. *Lab on a Chip* 9(24), 3549-3556.
- 580 Boysen, R.I., Schwarz, L.J., Li, S., Chowdhury, J., Hearn, M.T., 2014. *Microsyst. Technol.*  
581 20(10-11), 2037-2043.
- 582 Cauley, J.A., Lucas, F.L., Kuller, L.H., Stone, K., Browner, W., Cummings, S.R., 1999. *Ann.*  
583 *Intern. med.* 130(4), 270-277.
- 584 Chen, L., Wang, X., Lu, W., Wu, X., Li, J., 2016. *Chem. Soc. Rev.* 45(8), 2137-2211.
- 585 Chen, Y., Liu, Y., Shen, X., Chang, Z., Tang, L., Dong, W.-F., Li, M., He, J.-J., 2015. *Sensors*  
586 15(12), 29877.
- 587 Chianella, I., Piletsky, S.A., Tothill, I.E., Chen, B., Turner, A.P.F., 2003. *Biosens. Bioelectron.*  
588 18(2-3), 119-127.
- 589 Choi, K.M., 2014. *Bio-Chemical Sensors based on Molecularly Imprinted Polymers; Soft*  
590 *Lithography, Microfabrication and Microfluidic Synthesis.* One Central Press
- 591 Eersels, K., van Grinsven, B., Ethirajan, A., Timmermans, S., Jiménez Monroy, K.L., Bogie,  
592 J.F.J., Punniyakoti, S., Vandenryt, T., Hendriks, J.J.A., Cleij, T.J., Daemen, M.J.A.P., Somers,  
593 V., De Ceuninck, W., Wagner, P., 2013. *ACS Appl. Mater. Interfaces* 5(15), 7258-7267.
- 594 Fitzgerald, R.L., Griffin, T.L., Herold, D.A., 2010. *Methods Mol. Biol.* 603, 489-500.
- 595 Fuchs, Y., Soppera, O., Mayes, A.G., Haupt, K., 2013. *Adv. Mater.* 25(4), 566-570.
- 596 Gates, B.D., Xu, Q., Love, J.C., Wolfe, D.B., Whitesides, G.M., 2004. *Annu. Rev. Mater. Res.*  
597 34, 339-372.
- 598 Gooding, J.J., 2002. *Electroanal.* 14(17), 1149-1156.
- 599 Grieten, L., Janssens, S., Ethirajan, A., Bon, N.V., Ameloot, M., Michiels, L., Haenen, K.,  
600 Wagner, P., 2011. *Phys. Status Solidi A* 208(9), 2093-2098.
- 601 Hartl, A., Schmich, E., Garrido, J.A., Hernando, J., Catharino, S.C., Walter, S., Feulner, P.,  
602 Kromka, A., Steinmuller, D., Stutzmann, M., 2004. *Nat. Mater.* 3(10), 736-742.
- 603 Hernando, J., Pourrostami, T., Garrido, J.A., Williams, O.A., Gruen, D.M., Kromka, A.,  
604 Steinmüller, D., Stutzmann, M., 2007. *Diam. Relat. Mater.* 16(1), 138-143.
- 605 Hutter, N.A., Steenackers, M., Reitingner, A., Williams, O.A., Garrido, J.A., Jordan, R., 2011.  
606 *Soft Matter* 7(10), 4861-4867.
- 607 Hyde, Z., Flicker, L., McCaul, K.A., Almeida, O.P., Hankey, G.J., Chubb, S.P., Yeap, B.B.,  
608 2012. *Cancer Epidem. Biomar.* 21(8), 1319-1329.
- 609 Jin, H., Lin, J., Fu, L., Mei, Y.F., Peng, G., Tan, X., Wang, D.M., Wang, W., Li, Y.G., 2007.  
610 *Biochem. Cell Biol.* 85(2), 246-251.
- 611 Kamra, T., Chaudhary, S., Xu, C., Johansson, N., Montelius, L., Schnadt, J., Ye, L., 2015. *J.*  
612 *Colloid Interface Sci.* 445, 277-284.

613 Kellens, E., Bové, H., Conradi, M., D'Olieslaeger, L., Wagner, P., Landfester, K., Junkers, T.,  
614 Ethirajan, A., 2016. *Macromolecules* 49(7), 2559-2567.

615 Lavine, B.K., Westover, D.J., Kaval, N., Mirjankar, N., Oxenford, L., Mwangi, G.K., 2007.  
616 *Talanta* 72(3), 1042-1048.

617 LeJeune, J., Spivak, D.A., 2007. *Anal. Bioanal. Chem.* 389(2), 433-440.

618 Linares, A.V., Falcimaigne - Cordin, A., Gheber, L.A., Haupt, K., 2011. *Small* 7(16), 2318-  
619 2325.

620 Liss, M., Petersen, B., Wolf, H., Prohaska, E., 2002. *Anal. Chem.* 74(17), 4488-4495.

621 Liu, H., Ni, T., Mu, L., Zhang, D., Wang, J., Wang, S., Sun, B., 2018. *Sens. Actuator B:*  
622 *Chem.* 256, 1038-1044.

623 Peeters, M., Troost, F., van Grinsven, B., Horemans, F., Alenus, J., Murib, M.S., Keszthelyi,  
624 D., Ethirajan, A., Thoelen, R., Cleij, T., 2012. *Sens. Actuator B: Chem.* 171, 602-610.

625 Peeters, M., Troost, F.J., Mingels, R.H., Welsch, T., van Grinsven, B., Vranken, T.,  
626 Ingebrandt, S., Thoelen, R., Cleij, T.J., Wagner, P., 2013. *Anal. Chem.* 85(3), 1475-1483.

627 Pérez-Moral, N., Mayes, A.G., 2004. *Anal. Chim. Acta* 504(1), 15-21.

628 Piletsky, S.A., Alcock, S., Turner, A.P.F., 2001. *Trends Biotechnol.* 19(1), 9-12.

629 Reimhult, K., Yoshimatsu, K., Risveden, K., Chen, S., Ye, L., Krozer, A., 2008. *Biosens.*  
630 *Bioelectron.* 23(12), 1908-1914.

631 Rubio-Retama, J., Hernando, J., López-Ruiz, B., Härtl, A., Steinmüller, D., Stutzmann, M.,  
632 López-Cabarcos, E., Antonio Garrido, J., 2006. *Langmuir* 22(13), 5837-5842.

633 Ruigrok, V.J., Levisson, M., Eppink, M.H., Smidt, H., van der Oost, J., 2011. *Biochem. J.*  
634 436(1), 1-13.

635 Sellergren, B., 2000. *Molecularly Imprinted Polymers. Man-Made Mimics of Antibodies and*  
636 *their Application in Analytical Chemistry.* Elsevier Science, Amsterdam, The Netherlands.

637 Sellergren, B., Allender, C., 2005. *Adv. Drug Deliv. Rev.* 57(12), 1733-1741.

638 Steenackers, M., Jordan, R., Küller, A., Grunze, M., 2009. *Adv. Mater.* 21(28), 2921-2925.

639 Svenson, J., Nicholls, I.A., 2001. *Anal. Chim. Acta* 435(1), 19-24.

640 Taieb, J., Mathian, B., Millot, F., Patricot, M.C., Mathieu, E., Queyrel, N., Lacroix, I.,  
641 Somma-Delpero, C., Boudou, P., 2003. *Clin. Chem.* 49(8), 1381-1395.

642 Tan, Y., Jing, L., Ding, Y., Wei, T., 2015. *Appl. Surf. Sci.* 342, 84-91.

643 Thieme, D., Hemmersbach, P., 2009. *Doping in sports.* Springer Science & Business Media.

644 Tretjakov, A., Syritski, V., Reut, J., Boroznjak, R., Öpik, A., 2016. *Anal. Chim. Acta* 902,  
645 182-188.

646 Vaihinger, D., Landfester, K., Kräuter, I., Brunner, H., Tovar, G.E.M., 2002. *Macromol.*  
647 *Chem. Phys.* 203(13), 1965-1973.

648 van Grinsven, B., Vanden Bon, N., Grieten, L., Murib, M., Janssens, S.D., Haenen, K.,  
649 Schneider, E., Ingebrandt, S., Schoning, M.J., Vermeeren, V., Ameloot, M., Michiels, L.,  
650 Thoelen, R., De Ceuninck, W., Wagner, P., 2011. *Lab Chip* 11(9), 1656-1663.

651 Vera, F., Zenuto, R.R., Antenucci, C.D., Busso, J.M., Marín, R.H., 2011. *J. Exp. Zool. Part A*  
652 315A(9), 572-583.

653 Vermeeren, V., Grieten, L., Vanden Bon, N., Bijmens, N., Wenmackers, S., Janssens, S.D.,  
654 Haenen, K., Wagner, P., Michiels, L., 2011. *Sens. Actuator B: Chem.* 157(1), 130-138.

655 Wackers, G., Vandenryt, T., Cornelis, P., Kellens, E., Thoelen, R., De Ceuninck, W., Losada-  
656 Perez, P., van Grinsven, B., Peeters, M., Wagner, P., 2014. *Sensors* 14(6), 11016-11030.

657 Wang, J., 2001. *Electroanal.* 13(12), 983.

658 Wang, Y., Gay, G.D., Botelho, J.C., Caudill, S.P., Vesper, H.W., 2014. *Clin. Chim. Acta* 436,  
659 263-267.

660 Weng, C.-H., Yeh, W.-M., Ho, K.-C., Lee, G.-B., 2007. *Sens. Actuator B: Chem.* 121(2),  
661 576-582.

662 Wenmackers, S., Vermeeren, V., vandeVen, M., Ameloot, M., Bijmens, N., Haenen, K.,  
663 Michiels, L., Wagner, P., 2009. *Phys. Status Solidi A* 206(3), 391-408.

664 Whitcombe, M., Vulfson, E., 2001. *Adv. Mater.* 13(7), 467-478.  
665 Wild, D., 2013. *The Immunoassay Handbook (Fourth Edition)*. Elsevier, Oxford.  
666 Yang, M., Gu, W., Sun, L., Zhang, F., Ling, Y., Chu, X., Wang, D., 2010. *Talanta* 81(1-2),  
667 156-161.  
668 Yang, Q., Li, J., Wang, X., Peng, H., Xiong, H., Chen, L., 2018a. *Biosens. Bioelectron.*  
669 Yang, Q., Wu, X., Peng, H., Fu, L., Song, X., Li, J., Xiong, H., Chen, L., 2018b. *Talanta* 176,  
670 595-603.  
671 Yang, W., Auciello, O., Butler, J.E., Cai, W., Carlisle, J.A., Gerbi, J.E., Gruen, D.M.,  
672 Knickerbocker, T., Lasseter, T.L., Russell, J.N., Jr., Smith, L.M., Hamers, R.J., 2002. *Nat.*  
673 *Mater.* 1(4), 253-257.  
674